



Doxorubicin-loaded micelles of amphiphilic diblock copolymer with pendant dendron improve antitumor efficacy: *In vitro* and *in vivo* studies

Siew Hui Voon^a, Chin Siang Kue^a, Toyoko Imae^{b,c,**}, Wen Shang Saw^d, Hong Boon Lee^d,
Lik Voon Kiew^a, Lip Yong Chung^{d,*}, Shin-ichi Yusa^e

^a Department of Pharmacology, Faculty of Medicine, University of Malaya, 50603 Kuala Lumpur, Malaysia

^b Department of Chemical Engineering, National Taiwan University of Science and Technology, 43 Section 4, Keelung Road, Taipei 10607, Taiwan

^c Graduate Institute of Applied Science and Technology, National Taiwan University of Science and Technology, 43 Section 4, Keelung Road, Taipei 10607, Taiwan

^d Department of Pharmacy, Faculty of Medicine, University of Malaya, 50603 Kuala Lumpur, Malaysia

^e Department of Materials Science and Chemistry, University of Hyogo, 2167 Shosha, Himeji, Hyogo 671-2280, Japan



ARTICLE INFO

Keywords:

Diblock copolymer micelles
Doxorubicin
Anticancer
Drug delivery
Biodistribution

ABSTRACT

Previously reported amphiphilic diblock copolymer with pendant dendron moieties ($P_{71}D_3$) has been further evaluated in tumor-bearing mice as a potential drug carrier. This $P_{71}D_3$ -based micelle of an average diameter of 100 nm was found to be biocompatible, non-toxic and physically stable in colloidal system up to 15 days. It enhanced the *in vitro* potency of doxorubicin (DOX) in 4T1 breast tumor cells by increasing its uptake, by 3-fold, compared to free DOX. In 4T1 tumor-bearing mice, the tumor growth rate of $P_{71}D_3$ /DOX (2 mg/kg DOX equivalent) treated group was significantly delayed and their tumor volume was significantly reduced by 1.5-fold compared to those treated with free DOX. The biodistribution studies indicated that $P_{71}D_3$ /DOX enhanced accumulation of DOX in tumor by 5- and 2-fold higher than free DOX treated mice at 15 min and 1 h post-administration, respectively. These results suggest that $P_{71}D_3$ micelle is a promising nanocarrier for chemotherapeutic agents.

1. Introduction

Lack of tumor selectivity and high systemic toxicity of cancer chemotherapeutic drugs are the major hurdles in the current cancer chemotherapy (Voon et al., 2016; Yokoyama, 2006). In addition, increasing resistant type of tumors requires high doses of anticancer drugs, which in turn increase the systemic toxicity to the patient (Holohan et al., 2013; Voon et al., 2016). To overcome these hurdles, a targeted drug delivery system specific to the tumor site is expected to keep the dose at minimum and reduce toxicity, via high local drug concentration through enhanced permeation and retention effect (Bertrand et al., 2014; Maeda et al., 2000). Thus, nanocarriers for drug delivery have emerged in the field of cancer therapy in the past decades (Voon et al., 2014).

Polymer micelles have been extensively studied for their applications to deliver various drugs including chemotherapeutics, contrast agents, proteins, plasmid DNA and most recently siRNA (Kataoka et al., 2001; Nishiyama and Kataoka, 2006; Osada et al., 2009). The advantages of polymeric micelles as delivery agents are two-fold: the hydrophobic core serves as a solubilization depot for drugs with poor

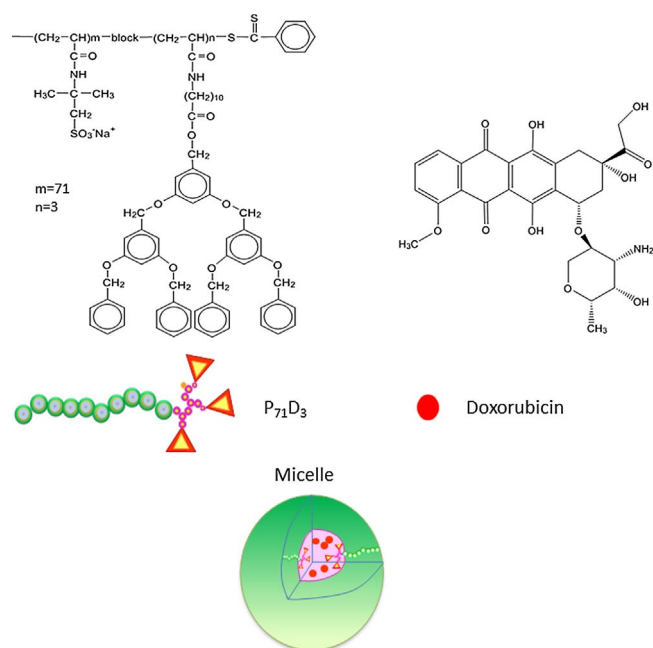
aqueous solubility; while the hydrophilic shell provides protection to limit opsonin adsorption in order to maintain better blood stability (Lu and Park, 2013). However, these polymeric micelle systems may have insufficient drug loading capacity, inadequate binding and uptake by cells (Owen et al., 2012).

Currently, there are a few polymer micelles that are in clinical trials, including doxorubicin (DOX)-encapsulated poly(ethylene glycol) (PEG)-poly(propylene oxide) (PPO)-PEG (Pluronic) micelles (SP1049C) in phase III (Armstrong et al., 2006), paclitaxel (PTX)-encapsulated PEG-polyaspartate block copolymer micelle (NK105) in phase II (Hamaguchi et al., 2005; Matsumura and Kataoka, 2009), and cisplatin-incorporated PEG-polyglutamate block copolymer micelle (NC-6004) in phase II (Matsumura and Kataoka, 2009; Uchino et al., 2005). These proved that polymer micelles are of potential clinical use as drug delivery system.

Previously, we reported a DOX loaded self-assembly micelle prepared from an amphiphilic diblock copolymer with pendant dendron ($P_{71}D_3$) for enhanced tumor cellular uptake (Viswanathan et al., 2016). The $P_{71}D_3$ polymers consist of a linear polyelectrolyte chain and a hydrophobic block carrying a pendant benzyloxy-type dendritic moiety

* Corresponding author.

** Corresponding author at: Department of Chemical Engineering, National Taiwan University of Science and Technology, 43 Section 4, Keelung Road, Taipei 10607, Taiwan.
E-mail addresses: imae@mail.ntust.edu.tw (T. Imae), chungly@um.edu.my (L.Y. Chung).



Scheme 1. Chemical structure of P₇₁D₃ and Doxorubicin, schematic representation of P₇₁D₃/DOX.

are able to self-assemble into spherical micelles (Yusa et al., 2011). This assembling phenomenon is thermodynamically controlled and stabilized, causing the hydrophobic moieties (blocks) to aggregate and form the hydrophobic micelle core. While the hydrophilic polyelectrolyte chains form the outer hydrophilic shells. The hydrophobic DOX molecules are then entrapped in the large cavity, within and between hydrophobic dendron moieties in the micelle core (Scheme 1). The P₇₁D₃ micelles were found to achieve a high drug loading capacity of 95% and increased uptake of DOX by 2-fold in tumor cells compared to free DOX (Viswanathan et al., 2016). However, extreme dilutions by blood upon intravenous administration of micellar solution may cause the polymeric micelles to prematurely deform and disassemble; leading to leakage and burst release of loaded drugs (Kulthe et al., 2012). Therefore, *in vivo* studies are required to evaluate the behavior of this delivery system in the body.

In the present work, we further evaluate the antitumor efficacy of P₇₁D₃-DOX in 4T1 breast cancer model *in vitro* and *in vivo*. Particle stability, biocompatibility, tumor cellular uptake and trafficking, tumor growth inhibition in 4T1 tumor-bearing mice, *in vivo* noninvasive imaging and biodistribution were investigated. Syngeneic murine mammary tumor model (4T1 breast cancer model) was adopted in this study as it closely mimics human late stage breast cancer (Tao et al., 2008).

2. Experimental section

2.1. Materials

The diblock copolymer P₇₁D₃ was the same sample as that previously synthesized (Osawa et al., 2013; Yusa et al., 2011). DOX was kindly donated by Prof. H. C. Tsai, National Taiwan University of Science and Technology, Taiwan. ProLong Gold Antifade Mountant with 4',6-diamidino-2-phenylindole (DAPI) was purchased from Molecular Probes, Invitrogen (Eugene, OR, USA). Other reagents were commercially available. Deionized ultrapure (ELGA PURELAB flex 3) water with a resistivity of 18.2 MΩ·cm was used throughout all syntheses and measurements.

2.2. Preparation of doxorubicin-loaded P₇₁D₃ micelles

Doxorubicin-loaded P₇₁D₃ micelles were prepared according to the method reported previously (Viswanathan et al., 2016). P₇₁D₃ (0.5 mg) and DOX (0.1 mg) were dissolved in water (5 ml). The mixture was allowed to stand overnight at room temperature to achieve complete dissolution. The aqueous solutions (5 ml) were then dialyzed against water using a regenerated cellulose dialysis tube (MWCO of 6000–8000 g mol⁻¹) over 32 h at room temperature until all free DOX was removed. To ensure complete removal of free DOX, the dialysis medium was changed every 2 h and measured with UV–vis spectrophotometer until the absorbance of DOX at 480 nm became negligible. The P₇₁D₃ micelles/DOX in aqueous solution were used directly for further physicochemical characterization experiments.

2.3. Physicochemical properties of P₇₁D₃ micelles: particle size, particle stability and zeta potential

The mean particle size and the size distribution of the P₇₁D₃ micelle were measured by applying the dynamic light scattering principle using a Malvern NanoSeries ZetaSizer. A volume of 50 μl of 1 mg/ml micelle was added to 3 ml of water and size measurement was then performed.

To evaluate the stability of the P₇₁D₃ micelle in a stock solution, the size of micelle was monitored for 15 days at ambient room temperature (27 °C) to analyze cluster formation. The sampling intervals for the measurements were day 1, 2, 6, 8, 10, 13 and 15.

The zeta potential of the P₇₁D₃ micelle was also determined by applying the principle of electrophoretic mobility under an electric field using a Malvern NanoSeries ZetaSizer. Zeta potential is related to the surface charge of the micelles and influence their interactions with cellular membranes. The size and zeta potential measurements of the P₇₁D₃ micelles were determined in triplicate.

2.4. *In vitro* cytotoxicity assay

Aqueous stock solutions of P₇₁D₃ (100 μg/ml polymer) and P₇₁D₃/DOX (95 μg/ml DOX equivalent polymer) were prepared. The 4T1 cells were grown and maintained in Roswell Park Memorial Institute (RPMI) medium supplemented with 10% fetal bovine serum (FBS) and 1% penicillin-streptomycin at 37 °C in a 5% CO₂ humidified chamber. 4T1 cells were seeded into 96-well plates at 5000 cells/well and were incubated overnight to allow cells to adhere before polymer samples were introduced. Polymer samples were diluted in culture medium and added to the cells to give final concentrations ranging from 0.156 to 1.25 μM DOX equivalent. The cells were then incubated for 24 h at 37 °C in 5% CO₂ before cell viability was assessed using the MTT assay (Kiew et al., 2017). Ten microliters of 3-(4,5-dimethylthiazol-2-yl)-2,5-diphenyl tetrazolium bromide (MTT) (5 mg/ml in phosphate buffered saline (PBS)) was added to each well and incubated for 3 h. The supernatant was carefully removed, and replaced with 100 μl of dimethylsulfoxide to dissolve the purple formazan crystal. The optical density of each well was measured at 570 nm using a microplate spectrophotometer. The viability of the cells in response to the treatment of polymeric micelle samples was calculated using the following equation:

$$\text{Percentage(\%)} \text{ of cell viability} = \left(\frac{\text{OD treated}}{\text{OD control}} \right) \times 100$$

Cell viability in the presence of a solvent control (PBS) was determined concurrently and three independent experiments were carried out.

2.5. Cellular internalization and subcellular localization of free DOX and P₇₁D₃/DOX micelles in 4T1 cancer cells

2.5.1. Cellular uptake study

The uptake of P₇₁D₃/DOX and free DOX by 4T1 cells was determined using flow cytometry (Viswanathan et al., 2016). First, the cells (1.5 × 10⁵ cells/well) were seeded in 12-well culture plates and incubated at 37 °C in a 5% CO₂ humidified chamber for 24 h to allow for cell adherence. Then, the cells were treated with P₇₁D₃/DOX or free DOX (1 µg/ml DOX equivalent) with 2 h incubation. After being incubated for 2 h, the treated cells were washed 2 times with cold PBS, trypsinized and transferred to tubes and centrifuged. The cells were re-suspended in 0.5 ml of PBS containing 0.5% FBS for flow cytometric analysis on a BD FACS Canto II flow cytometer (Becton Dickinson, San Jose, CA, USA) equipped with a 488 nm argon laser and a 670 nm long pass filter to detect the fluorescence emitted by the DOX taken up by the cells. Data from 10,000 cells were collected and analyzed using FACS DIVA analysis software (Becton Dickinson). The cellular uptake experiments were repeated three times.

2.5.2. Subcellular localization study

The procedure for confocal microscopy was as follows: 4T1 cells (2 × 10⁵ cells/well) in complete culture medium were seeded on glass coverslips (22 × 22 mm), placed in 6-well plates and incubated for 24 h at 37 °C in a 5% CO₂ humidified chamber. The cells were treated with P₇₁D₃/DOX (1 µg/ml DOX equivalent) and free DOX (1 µg/ml) for 2 h at 37 °C. The cells were fixed with 4% paraformaldehyde on a glass coverslip for 10 min at 37 °C and then rinsed twice with PBS. Fixed cells on glass coverslips were mounted on glass slides with mounting medium containing DAPI. Cellular uptake of the nanoparticles was observed with a confocal laser scanning microscope using a 63 × oil immersion objective (Leica TCS SP5 II, Leica Microsystems, Wetzlar, Mannheim, Germany). The DAPI dye was excited using a 405 nm diode laser and had its emission detected between 414 and 481 nm on the photomultiplier tube (PMT). DOX was excited using a 488 nm argon laser and had their emissions detected 590–720 nm on the PMT detector. All scans were performed in an independent sequential mode to avoid spectral overlap during acquisitions. Images were captured using the Leica LAS-AF image capture software (Lim et al., 2010).

2.6. Trafficking of P₇₁D₃/DOX micelles

To assess the effect of low temperature on the uptake of P₇₁D₃/DOX micelles and free DOX, the flow cytometric cellular uptake studies were repeated based on the procedures described above, except the cells were treated with P₇₁D₃/DOX micelles or free DOX for 2 h at 4 and 37 °C.

The uptake mechanisms of the P₇₁D₃/DOX micelles and free DOX were studied by treating the cells with different endocytosis inhibitors for 30 min at 37 °C, including amiloride at 10 µM, genistein at 100 µM or phenylarsine oxide at 2 µM. These inhibiting drugs were selected based on their ability to inhibit specific steps in the endocytic pathway. Inhibitors were then removed and the cells were washed two times with PBS. Following this, flow cytometric cellular uptake studies were repeated based on the procedures described previously (Viswanathan et al., 2016). Three independent experiments were carried out.

2.7. Hemo-biocompatibility assay

2.7.1. Hemolysis study

One hundred microliter aliquots of a 2% red blood cell (RBC) suspension were mixed with 100 µl of P₇₁D₃ micelles in sterile micro-centrifuge tubes to attain final concentrations ranging from 0 to 0.25 mg/ml. A positive control was also prepared by adding 100 µl of Triton X100 (1% v/v) to 100 µl aliquots of a 2% RBC suspension to produce 100% hemolysis. All samples (n = 3) were incubated for 5 h at

37 °C to allow hemolysis to take place (Kiew et al., 2010). The samples were then centrifuged for 10 min at 1000 × g, and the supernatants (100 µl) were transferred to 96-well plates to analyze hemoglobin release using spectrophotometric absorbance at 550 nm in an Infinite[®] M1000 Pro Tecan microplate reader (Männedorf, Meilen, Switzerland). The absorbance values of the respective samples were compared with the positive control, and the percent lysis was then calculated. The hemolysis experiments were repeated three times.

2.7.2. Red blood cell (RBC) aggregation study

The erythrocytes aggregation test was conducted according to Singhal and Ray (2002) with minor modifications. One hundred microliter aliquots of 2% RBC suspension in Ringer solution were mixed with 100 µl of P₇₁D₃ micelles in PBS at concentrations ranging from 0 to 0.25 mg/ml. For positive control, 100 µl of PBS was mixed with 100 µl of 2% RBC suspension in modified Ringer's solution that contains no sodium citrate. All the test and control samples (n = 3) were incubated for 2 h at 37 °C. After incubation, the samples were examined using Olympus CX31 microscope at 100 × magnification. Photomicrographs were taken using a Nikon Coolpix 4500 image recorder (Sumida-ku, Tokyo, Japan). The RBC aggregation studies were repeated three times.

2.8. Animal experiments

Female immunocompetent wild-type BALB/c mice (8–10 weeks old; body weight 18–20 g) were supplied by the Animal Experimental Unit, Faculty of Medicine, University of Malaya for the *in vivo* studies. The mice were maintained in the satellite animal facility of the Department of Pharmacology, Faculty of Medicine, University of Malaya. The mice were kept in a controlled environment with a 12-h light-dark cycle and free access to food and water. All animal experiments were performed in accordance with protocols and ethics that were approved by the Faculty of Medicine Institutional Animal Care and Use Committee of the University of Malaya (FOM IACUC) (Ethics Reference no. 2016-190607/PHAR/R/KLV).

2.8.1. *In vivo* anticancer efficacy study

To perform tumor transplantations, murine 4T1 breast cancer cells (5 × 10⁵) in 0.1 ml of RPMI medium were orthotopically injected into the mammary fat pads of BALB/c mice after their fur was shaved. When the tumor reached an average volume of approximately 100 mm³ (Lee et al., 2009), the mice were intravenously injected via tail vein with saline, free DOX, P₇₁D₃/DOX (2 mg/kg of free DOX), or with blank P₇₁D₃ micelles (0.2 mg/kg, which is equivalent to P₇₁D₃/DOX that contains 2 mg/kg of free DOX). All test samples were prepared in saline to achieve a volume of 0.2 ml per injection. The mice were randomly divided into 4 treatment groups (n = 7), as follows: (1) free DOX, (2) P₇₁D₃/DOX micelles, (3) blank P₇₁D₃ micelles and (4) normal saline. The tumor size was then monitored 3 times per week. Tumor volumes were measured using a caliper and calculated as follows:

$$\text{Tumor volume (mm}^3\text{)} = \left(L \times \frac{W^2}{2} \right)$$

where L is the longest dimension and W is the shortest dimension (Tomayko and Reynolds, 1989). The tumor volume was not allowed to exceed 1500 mm³ throughout the study for ethical reasons.

2.8.2. *In vivo* biodistribution studies

When the tumors established in the BALB/c mice reached an average volume of 100 mm³, the mice were randomly divided into 3 groups. P₇₁D₃/DOX micelles and free DOX (2 mg/kg DOX equivalent) in normal saline were intravenously injected via the tail vein into the mice. The mice (n = 3) were then sacrificed at predetermined time points (0, 0.25, 1, 6, 24 and 48 h post-administration of the free DOX or P₇₁D₃/DOX micelles). Major organs, including tumor tissues and the

kidneys, liver, lungs, skin, lymph nodes, spleen and eyes, were harvested and imaged using an *In Vivo* MS FX PRO (Carestream Molecular Imaging, Woodbridge, CT, USA) with an excitation filter at 488 nm and an emission filter at 580 nm to detect the fluorescence emitted by the DOX. The fluorescence intensities observed in each organ and tissue were quantified using Carestream Molecular Imaging software 5.0 (Woodbridge, CT, USA). Mice treated with saline under identical conditions were used as the controls (Voon et al., 2016).

2.8.3. *In vivo* toxicity profile of P₇₁D₃ micelles

The toxicity profiles of P₇₁D₃ micelles were determined after they were intravenously administered to the mice via tail vein at doses equivalent to 50 mg/kg. Toxicity was observed for 20 days by recording the symptoms, including inactivity, ruffled fur, behavior changes, and loss of body weight (Kue et al., 2015).

2.9. Statistical analysis

In vitro and *in vivo* experiments were performed to compare the efficacy of free DOX and P₇₁D₃/DOX micelles. Statistical analyses were performed using SPSS. One-Way ANOVA with Dunnett's Multiple Comparisons was used to compare means among the three groups of samples. Student's *t*-tests were used to assess differences between two groups. The mean differences were considered statistically significant when the *p* value was less than 0.05.

3. Results and discussion

3.1. Characterizations of P₇₁D₃ micelles

The amphiphilic diblock copolymers P₇₁D₃ (molecular weight of 2.60×10^6) self-assembled into micelles consisting of 104 molecules (Yusa et al., 2011). The P₇₁D₃ micelles had an average hydrodynamic diameter of 100 nm in PBS, and their size in PBS did not vary over a period of 15 days (Fig. 1). These results show that the micelles remained stable and did not aggregate.

The zeta potential of P₇₁D₃ micelles was approximately -10 mV and did not vary significantly over 15 days in PBS (Fig. 1). Our finding is similar to the zeta potential of micelles derived from other amphiphilic diblock copolymers including poly(oligoethylene glycol methyl ether methacrylate)-*b*-poly(4-vinylpyridine) (Topuzogullari et al., 2014), poly(ethylene glycol)-*b*-poly(benzyl malolactonate) (Loyer et al., 2013) and poly(ethylene glycol)-poly(β -L-malic acid)-campothecin-II (Yang et al., 2016) in the range of -8 to -16 mV.

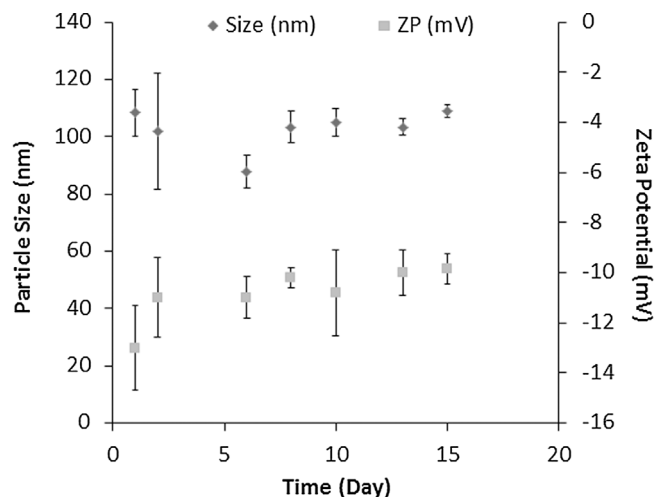


Fig. 1. Particle size and zeta potential (ZP) of P₇₁D₃ in phosphate buffered saline over 15 days. P₇₁D₃ remained stable in their size and zeta potential when kept at 27 °C. Data are expressed as mean \pm SD (*n* = 3).

The negative zeta potential on the micelles cause electrostatic repulsion among the particles and thus provide stability to the colloidal system against aggregation under physiological condition. In addition, particles with negative zeta potential are also able to reduce non-specific binding to normal cells including endothelial cells and to prolong their blood circulation time.

P₇₁D₃ micelles had effectively encapsulated DOX, with a high loading capacity of 95%, as reported in our previous publications. The amount of DOX release from P₇₁D₃ micelles was approximately 1.3-fold more abundant at a tumoral acidic pH of 5.5 compared to pH 7.4 (Viswanathan et al., 2016). Aromatic moiety in DOX may interact with the benzyloxy groups in the dendron side chain moiety of the block polymer. There could also be electrostatic interaction between the carboxylate terminal of block copolymer with the ammonium ion in DOX. These interactions may influence the DOX release. As the pKa of carboxylate in the polymer is around 6, it is likely to protonate at pH 5.5 and therefore loses the electrostatic interaction with the ammonium ion of DOX. This could explain the higher DOX release at the tumoral pH of 5.5 compared to pH 7.4 (normal tissues).

3.2. P₇₁D₃/DOX micelles enhanced cytotoxicity of DOX on 4T1 tumor cells

The 4T1 cancer cell viability following treatment was determined 24 h later using the MTT assay (Fig. 2). The P₇₁D₃/DOX micelles exhibited enhanced cytotoxicity, with a half maximal inhibitory concentration (IC₅₀) of 0.12 μ M (0.065 μ g/ml) DOX equivalent compared with free DOX (IC₅₀ = 0.2 μ M or 0.109 μ g/ml) under identical conditions. Our IC₅₀ value for free DOX was within the range of IC₅₀ found in the literature from 0.025 to 2.7 μ M (Zeng et al., 2014). This confirms that the P₇₁D₃/DOX micelles have a higher potency compared with free DOX. Additionally, the IC₅₀ value of P₇₁D₃/DOX micelles is also lower compared to other DOX loaded amphiphilic diblock polymeric micelles reported previously such as poly(ethylene glycol)-poly(ϵ -caprolactone) micelles (0.94 μ g/ml) (Sun et al., 2014) and poly(ethylene glycol)-polyamide amine micelles (0.086 μ g/ml) (Sun et al., 2013). As a control, cells treated with up to 10 μ g/ml P₇₁D₃ micelles showed no reduction in cell viability (data not shown), where the amount of P₇₁D₃ was approximately 16-fold higher than that in P₇₁D₃/DOX with 1.25 μ M DOX equivalent. This implies that the observed cytotoxicity of P₇₁D₃/DOX is because of the DOX in the P₇₁D₃ micelles. The higher cytotoxic potency of the P₇₁D₃/DOX micelles corresponds to their higher cellular uptake compared with free DOX, as described below.

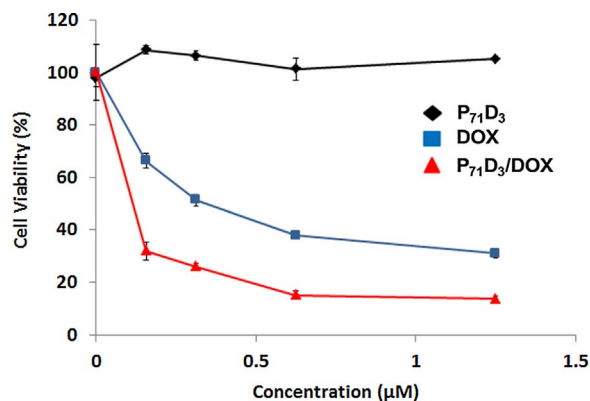


Fig. 2. The effect of P₇₁D₃/DOX, DOX and P₇₁D₃ on the viability of 4T1 cancer cells at 37 °C and 24 h incubation. The concentration refers to DOX and DOX equivalent for free DOX and P₇₁D₃/DOX micelles, respectively. For P₇₁D₃ micelles, the amount of P₇₁D₃ is equivalent to that in P₇₁D₃/DOX micelles, and the concentration refers DOX equivalent. Data are represented as the mean \pm SD (*n* = 3).

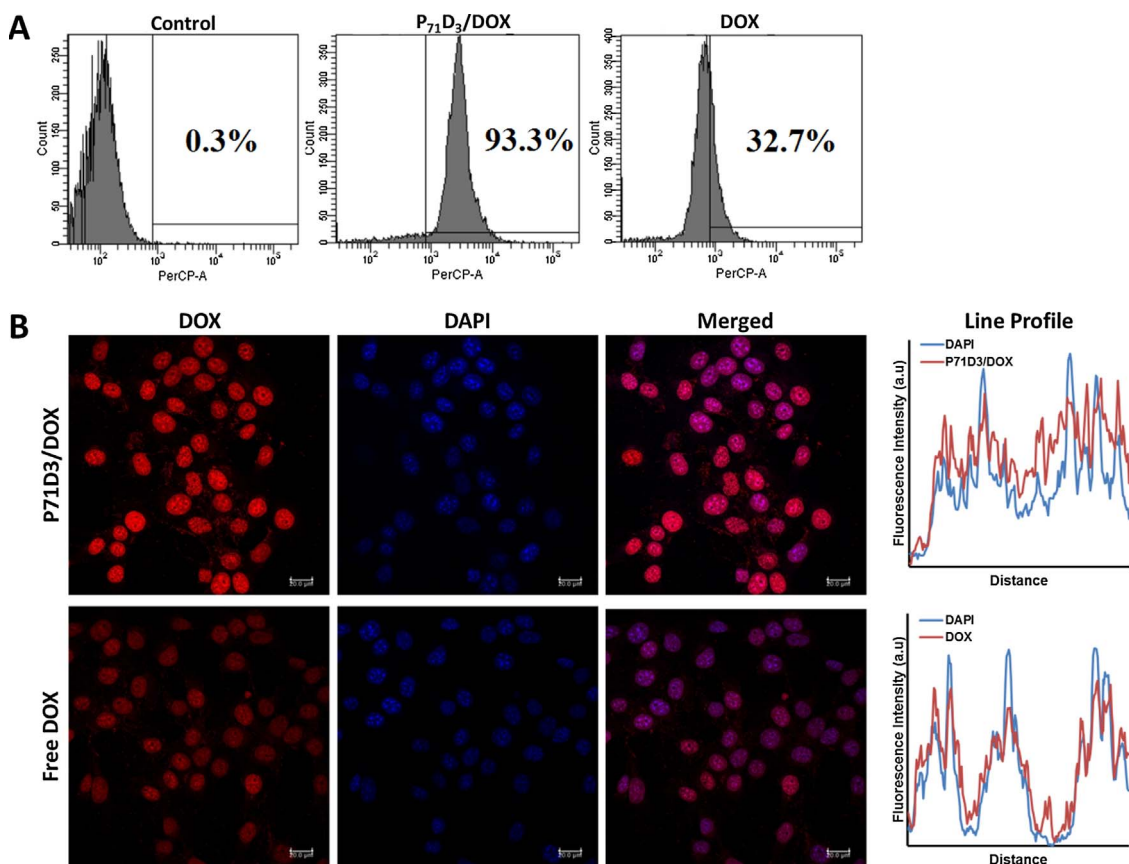


Fig. 3. Cellular uptake of $P_{71}D_3/DOX$ and DOX in 4T1 cells using flow cytometry and confocal microscopy after 2 h incubation at 37 °C. (A) Percentage of cellular uptake of $P_{71}D_3/DOX$ and DOX at 1 $\mu\text{g}/\text{ml}$ DOX equivalent measured using flow cytometry, and (B) Confocal microscopic images and line profiles of $P_{71}D_3/DOX$ and DOX at 1 $\mu\text{g}/\text{ml}$ DOX equivalent on DAPI-labelled cells. Scale bar: 20 μm .

3.3. $P_{71}D_3/DOX$ micelles enhanced uptake of DOX by tumor cells

Cellular uptake of the $P_{71}D_3/DOX$ micelles and free DOX by 4T1 cancer cells was quantified with flow cytometry based on the fluorescence of DOX. The $P_{71}D_3/DOX$ micelles exhibited the highest cellular uptake of 93% after incubation for 2 h compared with the free DOX (33%) (Fig. 3A), which is consistent with its high cellular uptake ($\approx 99\%$) by MDA-MB-231 human breast cancer cells (Viswanathan et al., 2016). However, this is contrary to the results reported by Prabakaran et al. (2009), where the 4T1 cellular uptake of free DOX was greater than poly(L-aspartate-doxorubicin)-*b*-poly(ethylene glycol) copolymer micelles conjugated with active targeting molecules, folic acid.

The cellular uptake of DOX in $P_{71}D_3$ micelles and free DOX at an equivalent dose in the 4T1 cells was also evaluated with confocal microscopy. The red fluorescence of DOX observed in the 4T1 cells treated with $P_{71}D_3/DOX$ micelles was brighter than in the cells treated with free DOX (Fig. 3B). The results from cellular uptake suggested an enhanced accumulation of $P_{71}D_3/DOX$ micelles in the cells.

In cells treated with $P_{71}D_3/DOX$ micelles, high intensities of red fluorescence were found mainly colocalized in the nuclear compartment that stained with DAPI (blue fluorescence), but less in the cytoplasm, as shown in the partial overlap DAPI and DOX topographic lines in the colocalization line profile in Fig. 3B. Conversely, in cells treated with free DOX, the red DOX fluorescence intensity was found only in the nuclear compartment, but not in the cytoplasm as the DAPI and DOX topographic lines are almost identical and overlapped with each other. These findings are consistent with and supported by our previous report (Viswanathan et al., 2016) on the trafficking of $P_{71}D_3/DOX$. Thus, it is suggested that the DOX is released from the $P_{71}D_3$ micelles in the tumor lysosomes upon cellular uptake, and then diffuses to the

nucleus to exert its cytotoxic effect (Viswanathan et al., 2016).

3.4. Cellular uptake mechanisms and pathway studies

The 4T1 cells were treated with $P_{71}D_3/DOX$ and free DOX to determine the cellular uptake mechanism, intracellular localization and accumulation. Endocytosis is one of the main uptake pathways for various extracellular materials and nanodrugs. Almost all endocytic pathways are energy-dependent processes that can be inhibited at low temperature, 4 °C. Fig. 4 shows that the incubation of the 4T1 cells with $P_{71}D_3/DOX$ at 4 °C for 2 h had caused an approximately 30% decrease in uptake compared with the cells incubated at 37 °C, as measured by flow cytometry. This indicated that the internalization of $P_{71}D_3/DOX$ into 4T1 cells occurred via an energy-dependent process. Our findings are consistent with Zeng et al. (2012) where the incubation of MCF-7/ADR cells with DOX-loaded polyester-based hyperbranched dendritic-linear based nanoparticles at 4 °C had resulted in a 32.5% decrease in DOX accumulation compared to cells incubated at 37 °C. Our previous study had reported a greater decrease of approximately 90% in DOX uptake at 4 °C in MDA-MD-231 cancer cells incubated with $P_{71}D_3/DOX$ compared to those treated at 37 °C. Therefore, the degree of the inhibition of cellular uptake by lowering the temperature varies according to cell lines.

The endocytic inhibitors used in this study, including amiloride hydrochloride, genistein and phenylarsine oxide, did not show significant inhibition effect on the internalization of $P_{71}D_3/DOX$ in 4T1 cells, when incubated at 37 °C for 2 h (Fig. 4). However, copolymer micelles and dendritic nanoparticles had been reported to be taken up into the cells via clathrin- and macropinocytosis-mediated pathways in breast tumor cells (Zeng et al., 2014, 2012).

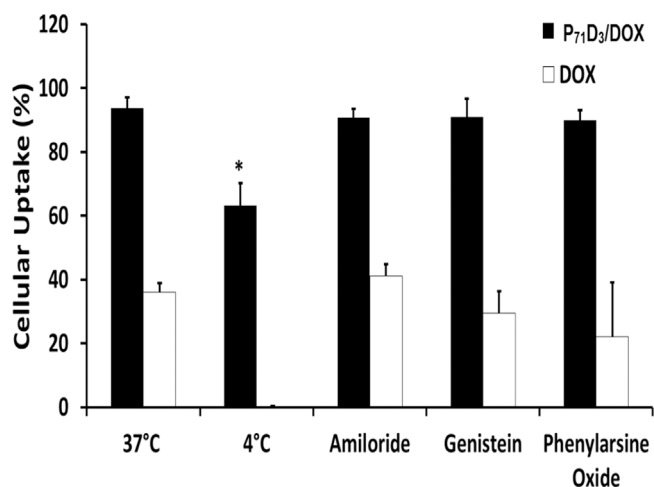


Fig. 4. Effect of temperature (37 and 4 °C) and endocytic inhibitors on accumulation of $P_{71}D_3$ /DOX and DOX in 4T1 cells. Cells were untreated (control and 4 °C) or pretreated with inhibitors for 30 min at 37 °C prior to addition of $P_{71}D_3$ /DOX and DOX (1 μ g/ml DOX equivalent). The fluorescence signal was measured using flow cytometry following incubation at 37 °C in all cases except the one labeled 4 °C for 2 h. Data represents the mean \pm SD (n = 3). * p < 0.05 compared to control.

3.5. Biocompatibility of $P_{71}D_3$ micelles: hemolysis tests and red blood cells aggregation test

Hemo-biocompatibility is important to prevent complications such as hemolytic anemia when nanoparticles are administered *in vivo*. After being incubated for 5 h with the nanoparticles, a small degree of hemolysis of red blood cells was observed and displayed a plateau at approximately 12% in the $P_{71}D_3$ micelles at concentrations up to 0.25 mg/ml (Fig. 5). These levels are tolerable (Ilium, 1998) because these substances are considered to be non-hemolytic when less than 15% of red blood cells are lysed in these assays (Petersen et al., 2002; Richardson et al., 1999).

In the aggregation study, aggregates of red blood cells were not found in the cells treated with $P_{71}D_3$ only or negative control (PBS). Conversely, significant aggregates of red blood cells were found in cells treated with positive control (Data not shown). These results suggest that $P_{71}D_3$ micelles were hemo-biocompatible and appropriate for systemic administration.

Our finding is consistent with other polymer micelles, including poly(ethylene oxide)-block-poly(β benzyl-L-aspartate) micelles (Yu et al., 1998), monomethoxy poly(ethylene glycol)-poly(lactide) diblock copolymers micelles (Li et al., 2009) and amphiphilic copolymer poly

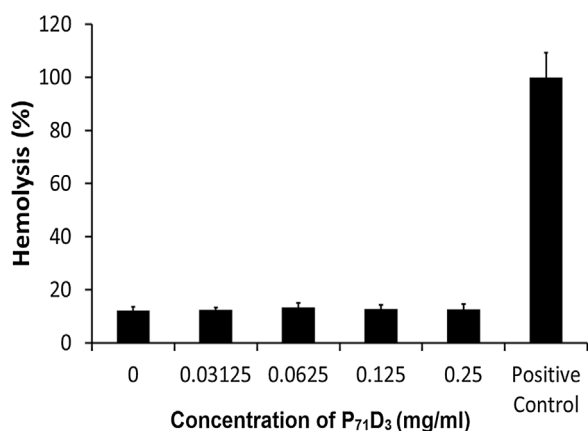


Fig. 5. Hemolysis test of $P_{71}D_3$. $P_{71}D_3$ is classified as non-hemolytic, as the hemolysis level was approximately 12% (less than 15%). Triton-X100 served as a positive control. Data represents the mean \pm SD (n = 3).

(*d,l*-lactide-co-2-methyl-2-carboxytrimethylenecarbonate) – *g*-poly(ethylene glycol) micelles (Lu et al., 2011), which were also reported to be compatible with red blood cells and did not exert hemolytic effect. Furthermore, the amount of $P_{71}D_3$ that was administered in this study was approximately 0.05 mg per mouse, and this amount would be rapidly diluted by the total blood volume in circulation (estimated to be 2 ml). Therefore, the degree of hemolysis that is caused by this minute amount of $P_{71}D_3$ is expected to be negligible, which has no significant difference compared to the negative or solvent control (0), as indicated in Fig. 5.

3.6. Animal model

3.6.1. Toxicity profile of $P_{71}D_3$ micelles

$P_{71}D_3$ micelles were administered at 50 mg/kg intravenously to the mice via the tail vein. Toxicity was evaluated using the Berlin test to analyze typical symptoms, including inactivity, ruffled fur, diarrhea, behavioral changes, and loss of body weight. No death or symptoms of toxicity was observed in the mice that treated with 50 mg/kg $P_{71}D_3$ micelles. Body weight changes of BALB/C mice over 17 days are provided in the supplementary material section (Fig. S1).

3.6.2. Antitumor efficacy study of $P_{71}D_3$ /DOX on 4T1 tumor

The tumor selectivity and antitumor effects of $P_{71}D_3$ /DOX were assessed and compared to free DOX in female BALB/c mice bearing 4T1 mammary tumors. Fig. 6 shows the tumor growth rate of all groups. The average tumor volume after administration of $P_{71}D_3$ /DOX, free DOX and blank $P_{71}D_3$ were clearly distinguishable from each other. The tumor growth rate of $P_{71}D_3$ /DOX-treated group was significantly delayed and the tumor volume was significantly reduced by 1.5- and 1.8-fold compared to those treated with free DOX and blank $P_{71}D_3$ micelles, respectively, from day-8 post treatment (p < 0.05, One-Way ANOVA). The group treated with free DOX showed increase in tumor growth and their growth rate was slightly delayed compared to the control group treated with blank $P_{71}D_3$ micelle (Fig. 6). All the mice were sacrificed when their tumor volume exceed 1500 mm³ for ethical reasons. These results indicate that the DOX-loaded in $P_{71}D_3$ micelles significantly inhibited the growth of 4T1 tumors in mice when compared to free DOX. Our results are consistent with that of Gao et al. (2005) where the tumor volume in mice treated with DOX-loaded micelles (3 mg/kg DOX equivalent) was significantly smaller than that treated with free DOX, although the tumor growth was not completely suppressed in both

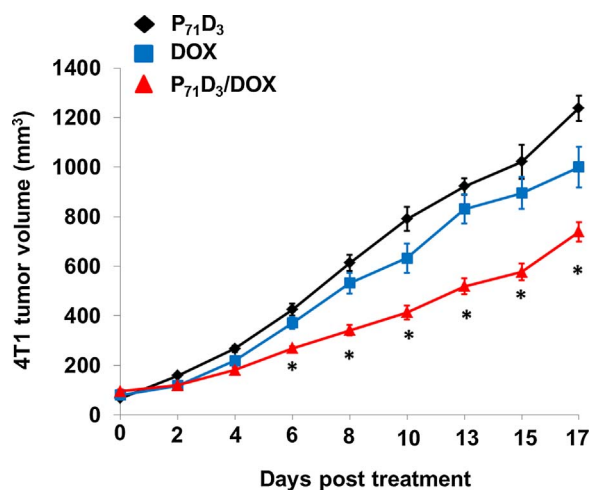


Fig. 6. *In vivo* anticancer efficacy of $P_{71}D_3$ /DOX micelles in 4T1 tumor-bearing mice. $P_{71}D_3$ /DOX micelles (2 mg/kg DOX equivalent) effectively suppressed 4T1 tumor growth compared to free DOX (2 mg/kg) and saline. Data represents the mean tumor volume \pm SEM (n = 7) for each group. * p < 0.05 compared to $P_{71}D_3$ or solvent control.

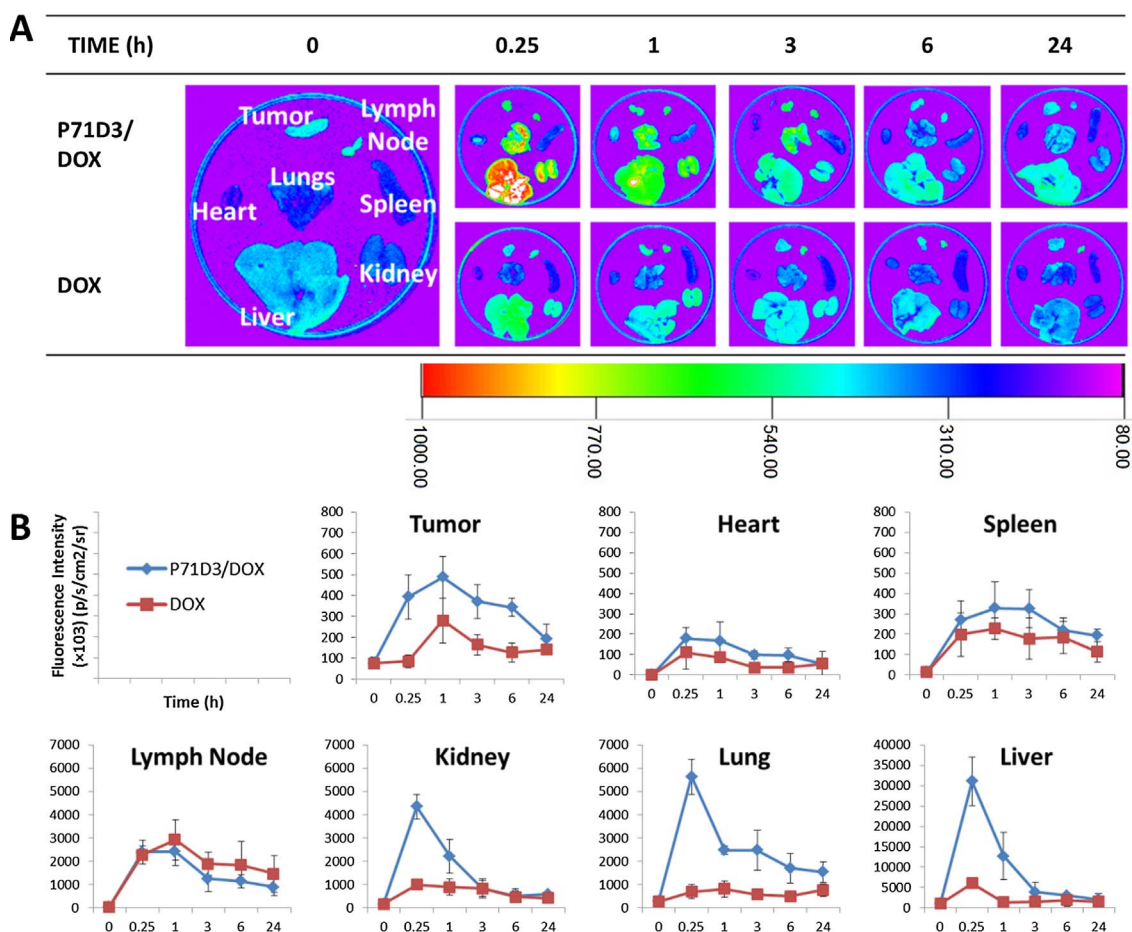


Fig. 7. *In vivo* biodistribution studies in 4T1 tumor-bearing mice. The mice were treated with a 2 mg/kg equivalent of DOX via the tail vein ($n = 3$). (A) Organs and tissues (tumor, heart, spleen, lymph node, kidney, lung and liver) were harvested, and (B) fluorescence intensities per centimeter squared per steradian ($\text{p/s/cm}^2/\text{sr}$) of each organ was recorded using an *in vivo* imager. Data represents mean \pm SD ($n = 3$) at each time point.

treated groups. Additionally, [Wei et al. \(2015\)](#) also reported that free DOX only moderately retarded tumor growth at 5 mg/kg whereas treatment with DOX-loaded amphiphilic dendrimer micelles significantly inhibited tumor growth.

No changes in the body weight of each group over time were observed throughout the antitumor study (data not shown). This indicates that there was no overall systemic toxicity caused by the formulations.

3.6.3. *In vivo* biodistribution studies

The biodistribution of $\text{P}_{71}\text{D}_3/\text{DOX}$ micelle and free DOX were monitored in 4T1 tumor-bearing mice for up to 24 h. A rapid accumulation and a significant increase of DOX-loaded micelles in tumors were observed compared to free DOX at 15 min and 1 h post-administration ([Fig. 7](#)). At 15 min post-administration, the fluorescence intensity of the tumors that were treated with $\text{P}_{71}\text{D}_3/\text{DOX}$ was approximately 5-fold higher ($393 \pm 106 \times (10^3) \text{ p/s/cm}^2/\text{sr}$) than the intensity observed in the mice that were treated with free DOX ($85 \pm 30 \times (10^3) \text{ p/s/cm}^2/\text{sr}$) ($p < 0.05$, Student's *t*-Test). The accumulation of $\text{P}_{71}\text{D}_3/\text{DOX}$ in tumor was highest at 1 h post-administration, when the fluorescence intensities of the mice treated with $\text{P}_{71}\text{D}_3/\text{DOX}$ ($487 \pm 99 \times (10^3) \text{ p/s/cm}^2/\text{sr}$) was 2-fold higher than the intensities in the group treated with free DOX ($281 \pm 108 \times (10^3) \text{ p/s/cm}^2/\text{sr}$) ($p < 0.05$, Student's *t*-Test). These results indicate that selective and rapid tumor accumulation of DOX was achieved when DOX was loaded in P_{71}D_3 micelles, and the maximal accumulation of $\text{P}_{71}\text{D}_3/\text{DOX}$ and free DOX occurred at 1 h post-administration.

A large amount of $\text{P}_{71}\text{D}_3/\text{DOX}$ was accumulated in the liver (approximately 20-fold more than in the tumor) and then in lung, kidney

and lymph node within the first 15 min post-administration ([Fig. 7A](#)), but these accumulations were dissipated swiftly in the subsequent monitoring period. A similar pattern but a significantly reduced amount was found for free DOX, where the accumulation peaked at 15 min in the liver and kidney and 1 h in the lungs. Swift clearance of both $\text{P}_{71}\text{D}_3/\text{DOX}$ and free DOX in these organs is typical of micelles and small molecular weight compounds. This also indicates that the accumulation in these organs was random and non-selective. [Kim et al. \(2009\)](#) reported similar finding where the DOX level in the liver and kidney was higher when compared to the tumor after administration of DOX-loaded micelles in ovarian tumor-xenografted mouse models.

Accumulation of $\text{P}_{71}\text{D}_3/\text{DOX}$ and free DOX was also observed in heart, spleen and lymph node at a much lower level ([Fig. 7](#)). There was no significant difference between the two samples in these organs. [Gao et al. \(2005\)](#) also reported that the DOX fluorescence in heart and spleen was at low level close to autofluorescence when the DOX micelles and free DOX were intravenously administered at 6 mg/kg DOX equivalent. We suggest that to improve the tumor targeting property and tumor selectivity of P_{71}D_3 based micelles, tumor targeting ligands such as folate and others could be conjugated to the surface of the micelles ([Kue et al., 2016](#)). Further understanding of the pharmacokinetics of the micelles may facilitate further optimization to improve delivery and minimize unwanted toxicity.

4. Conclusion

In conclusion, this study shows that P_{71}D_3 micelles are stable as a colloidal system up to 15 days, biocompatible, and enhance the uptake

of DOX in breast cancer cells by 3-folds compared to free DOX. Additionally, P₇₁D₃ micelles also increase accumulation of DOX in tumor tissue in 4T1 tumor-bearing mice *in vivo* by at least 2-fold and enhance its antitumor efficacy by 1.5-fold compared to free DOX in cancer chemotherapy. These suggest that P₇₁D₃ micelles could be a promising anticancer drug nanocarrier to achieve better treatment efficacy for chemotherapy.

Acknowledgement

We would like to thank HIR-MoHE grants (UM.C/625/1/HIR/MOHE/MED/17 and UM.C/625/1/HIR/MOHE/MED/33) for financial support.

Appendix A. Supplementary data

Supplementary data associated with this article can be found, in the online version, at <https://doi.org/10.1016/j.ijpharm.2017.10.023>.

References

- Armstrong, A., Brewer, J., Newman, C., Alakhov, V., Pietrzynski, G., Campbell, S., Corrie, P., Ranson, M., Valle, J., 2006. SP1049C as first-line therapy in advanced (inoperable or metastatic) adenocarcinoma of the oesophagus: a phase II window study. *J. Clin. Oncol.* 24 (18_suppl) (4080-4080).
- Bertrand, N., Wu, J., Xu, X., Kamaly, N., Farokhzad, O.C., 2014. Cancer nanotechnology: the impact of passive and active targeting in the era of modern cancer biology. *Adv. Drug Deliv. Rev.* 66, 2–25.
- Gao, Z.G., Lee, D.H., Kim, D.I., Bae, Y.H., 2005. Doxorubicin loaded pH-sensitive micelle targeting acidic extracellular pH of human ovarian A2780 tumor in mice. *J. Drug Target.* 13, 391–397.
- Hamaguchi, T., Matsumura, Y., Suzuki, M., Shimizu, K., Goda, R., Nakamura, I., Nakatomi, I., Yokoyama, M., Kataoka, K., Kakizoe, T., 2005. NK105, a paclitaxel-incorporating micellar nanoparticle formulation, can extend *in vivo* antitumor activity and reduce the neurotoxicity of paclitaxel. *Br. J. Cancer* 92, 1240–1246.
- Holohan, C., Van Schaeuybroeck, S., Longley, D.B., Johnston, P.G., 2013. Cancer drug resistance: an evolving paradigm. *Nat. Rev. Cancer* 13, 714–726.
- Ilium, L., 1998. Chitosan and its use as a pharmaceutical excipient. *Pharm. Res.* 15, 1326–1331.
- Kataoka, K., Harada, A., Nagasaki, Y., 2001. Block copolymer micelles for drug delivery: design, characterization and biological significance. *Adv. Drug Deliv. Rev.* 47, 113–131.
- Kiew, L.V., Cheong, S.K., Sidik, K., Chung, L.Y., 2010. Improved plasma stability and sustained release profile of gemcitabine via polypeptide conjugation. *Int. J. Pharm.* 391, 212–220.
- Kiew, L.V., Cheah, H.Y., Voon, S.H., Gallon, E., Movellan, J., Ng, K.H., Alpugan, S., Lee, H.B., Dumoulin, F., Vicent, M.J., 2017. Near-infrared activatable phthalocyanine-poly-L-glutamic acid conjugate: increased cellular uptake and light-dark toxicity ratio toward an effective photodynamic cancer therapy. *Nanomed-Nanotechnol* 13, 1447–1458.
- Kim, D., Gao, Z.G., Lee, E.S., Bae, Y.H., 2009. *In vivo* evaluation of doxorubicin-loaded polymeric micelles targeting folate receptors and early endosomal pH in drug-resistant ovarian cancer. *Mol. Pharm.* 6, 1353–1362.
- Kue, C.S., Kamkaew, A., Lee, H.B., Chung, L.Y., Kiew, L.V., Burgess, K., 2015. Targeted PDT agent eradicates TrkC expressing tumors via photodynamic therapy (PDT). *Mol. Pharm.* 12, 212–222.
- Kue, C.S., Kamkaew, A., Voon, S.H., Kiew, L.V., Chung, L.Y., Burgess, K., Lee, H.B., 2016. Tropomyosin receptor kinase C targeted delivery of a peptidomimetic ligand-photosensitizer conjugate induces antitumor immune responses following photodynamic therapy. *Sci. Rep.* 6, 37209.
- Kulthe, S.S., Choudhari, Y.M., Inamdar, N.N., Mourya, V., 2012. Polymeric micelles: authoritative aspects for drug delivery. *Des. Monomers Polym.* 15, 465–521.
- Lee, S.J., Park, K., Oh, Y.-K., Kwon, S.-H., Her, S., Kim, I.-S., Choi, K., Lee, S.J., Kim, H., Lee, S.G., Kim, K., Kwon, I.C., 2009. Tumor specificity and therapeutic efficacy of photosensitizer-encapsulated glycol chitosan-based nanoparticles in tumor-bearing mice. *Biomaterials* 30, 2929–2939.
- Li, X., Yang, Z., Yang, K., Zhou, Y., Chen, X., Zhang, Y., Wang, F., Liu, Y., Ren, L., 2009. Self-assembled polymeric micellar nanoparticles as nanocarriers for poorly soluble anticancer drug etaselen. *Nanoscale Res. Lett.* 4, 1502–1511.
- Lim, S.H., Thivierge, C., Nowak-Sliwinska, P., Han, J., Van Den Bergh, H., Wagnieres, G., Burgess, K., Lee, H.B., 2010. *In vitro* and *in vivo* photocytotoxicity of boron dipyrromethene derivatives for photodynamic therapy. *J. Med. Chem.* 53, 2865–2874.
- Loyer, P., Bedhouche, W., Huang, Z.W., Cammas-Marion, S., 2013. Degradable and biocompatible nanoparticles decorated with cyclic RGD peptide for efficient drug delivery to hepatoma cells *in vitro*. *Int. J. Pharm.* 454, 727–737.
- Lu, Y., Park, K., 2013. Polymeric micelles and alternative nanonized delivery vehicles for poorly soluble drugs. *Int. J. Pharm.* 453, 198–214.
- Lu, J., Owen, S.C., Shoichet, M.S., 2011. Stability of self-assembled polymeric micelles in serum. *Macromolecules* 44, 6002–6008.
- Maeda, H., Wu, J., Sawa, T., Matsumura, Y., Hori, K., 2000. Tumor vascular permeability and the EPR effect in macromolecular therapeutics: a review. *J. Control. Release* 65, 271–284.
- Matsumura, Y., Kataoka, K., 2009. Preclinical and clinical studies of anticancer agent-incorporating polymer micelles. *Cancer Sci.* 100, 572–579.
- Nishiyama, N., Kataoka, K., 2006. Current state, achievements, and future prospects of polymeric micelles as nanocarriers for drug and gene delivery. *Pharmacol. Ther.* 112, 630–648.
- Osada, K., Christie, R.J., Kataoka, K., 2009. Polymeric micelles from poly(ethylene glycol)-poly(amino acid) block copolymer for drug and gene delivery. *J. R. Soc. Interface* 6 (Suppl. 3), S325–S339.
- Osawa, K., Imae, T., Ujihara, M., Harada, A., Ochi, K., Ishihara, K., Yusa, S.-i., 2013. Preparation of amphiphilic diblock copolymers with pendant hydrophilic phosphorylcholine and hydrophobic dendron groups and their self-association behavior in water. *J. Polym. Sci. A Polym. Chem.* 51, 4923–4931.
- Owen, S.C., Chan, D.P., Shoichet, M.S., 2012. Polymeric micelle stability. *Nano Today* 7, 53–65.
- Petersen, H., Fechner, P.M., Martin, A.L., Kunath, K., Stolnik, S., Roberts, C.J., Fischer, D., Davies, M.C., Kissel, T., 2002. Polyethylenimine-graft-poly(ethylene glycol) copolymers: influence of copolymer block structure on DNA complexation and biological activities as gene delivery system. *Bioconjugate Chem.* 13, 845–854.
- Prabakaran, M., Graier, J.J., Pilla, S., Steeber, D.A., Gong, S., 2009. Gold nanoparticles with a monolayer of doxorubicin-conjugated amphiphilic block copolymer for tumor-targeted drug delivery. *Biomaterials* 30, 6065–6075.
- Richardson, S.C., Kolbe, H.V., Duncan, R., 1999. Potential of low molecular mass chitosan as a DNA delivery system: biocompatibility, body distribution and ability to complex and protect DNA. *Int. J. Pharm.* 178, 231–243.
- Singhal, J.P., Ray, A.R., 2002. Synthesis of blood compatible polyamide block copolymers. *Biomaterials* 23, 1139–1145.
- Sun, Y., Zou, W., Bian, S., Huang, Y., Tan, Y., Liang, J., Fan, Y., Zhang, X., 2013. Bioreducible PAA-g-PEG graft micelles with high doxorubicin loading for targeted antitumor effect against mouse breast carcinoma. *Biomaterials* 34, 6818–6828.
- Sun, L., Deng, X., Yang, X., Li, Z., Wang, Z., Li, L., Wu, Q., Peng, F., Liu, L., Gong, C., 2014. Co-delivery of doxorubicin and curcumin by polymeric micelles for improving antitumor efficacy on breast carcinoma. *RSC Adv.* 4, 46737–46750.
- Tao, K., Fang, M., Alroy, J., Sahagian, G.G., 2008. Imagable 4T1 model for the study of late stage breast cancer. *BMC Cancer* 8, 228.
- Tomayko, M.M., Reynolds, C.P., 1989. Determination of subcutaneous tumor size in athymic (nude) mice. *Cancer Chemother. Pharmacol.* 24, 148–154.
- Topuzogullari, M., Bulmus, V., Dalgakiran, E., Dinçer, S., 2014. pH- and temperature-responsive amphiphilic diblock copolymers of 4-vinylpyridine and oligoethyleneglycol methacrylate synthesized by RAFT polymerization. *Polymer* 55, 525–534.
- Uchino, H., Matsumura, Y., Negishi, T., Koizumi, F., Hayashi, T., Honda, T., Nishiyama, N., Kataoka, K., Naito, S., Kakizoe, T., 2005. Cisplatin-incorporating polymeric micelles (NC-6004) can reduce nephrotoxicity and neurotoxicity of cisplatin in rats. *Br. J. Cancer* 93, 678–687.
- Viswanathan, G., Hsu, Y.H., Voon, S.H., Imae, T., Siriviriyun, A., Lee, H.B., Kiew, L.V., Chung, L.Y., Yusa, S., 2016. A comparative study of cellular uptake and subcellular localization of doxorubicin loaded in self-assemblies of amphiphilic copolymers with pendant dendron by MDA-MB-231 human breast cancer cells. *Macromol. Biosci.* 16, 882–895.
- Voon, S.H., Kiew, L.V., Lee, H.B., Lim, S.H., Noordin, M.L., Kamkaew, A., Burgess, K., Chung, L.Y., 2014. *In vivo* studies of nanostructure-based photosensitizers for photodynamic cancer therapy. *Small* 10, 4993–5013.
- Voon, S.H., Tiew, S.X., Kue, C.S., Lee, H.B., Kiew, L.V., Misran, M., Kamkaew, A., Burgess, K., Chung, L.Y., 2016. Chitosan-coated poly(lactic-co-glycolic acid)-diiodinated boron-dipyrromethene nanoparticles improve tumor selectivity and stealth properties in photodynamic cancer therapy. *J. Biomed. Nanotechnol.* 12, 1431–1452.
- Wei, T., Chen, C., Liu, J., Liu, C., Posocco, P., Liu, X., Cheng, Q., Huo, S., Liang, Z., Fermeiglia, M., Pricl, S., Liang, X.-J., Rocchi, P., Peng, L., 2015. Anticancer drug nanomicelles formed by self-assembling amphiphilic dendrimer to combat cancer drug resistance. *Proc. Natl. Acad. Sci. U.S.A.* 112, 2978–2983.
- Yang, T., Li, W., Duan, X., Zhu, L., Fan, L., Qiao, Y., Wu, H., 2016. Preparation of two types of polymeric micelles based on poly(β -L-malic acid) for antitumor drug delivery. *PLoS One* 11, e0162607.
- Yokoyama, M., 2006. Polymeric Micelle Drug Carriers for Tumor Targeting Polymeric Drug Delivery I. American Chemical Society, pp. 27–39.
- Yu, B.G., Okano, T., Kataoka, K., Kwon, G., 1998. Polymeric micelles for drug delivery: solubilization and haemolytic activity of amphotericin B. *J. Control. Release* 53, 131–136.
- Yusa, S.-i., Shimada, Y., Imae, T., Morishima, Y., 2011. Self-association behavior in water of an amphiphilic diblock copolymer comprised of anionic and dendritic blocks. *Polym. Chem.* 2, 1815–1821.
- Zeng, X., Morgenstern, R., Nyström, A.M., 2014. Nanoparticle-directed sub-cellular localization of doxorubicin and the sensitization breast cancer cells by circumventing GST-Mediated drug resistance. *Biomaterials* 35, 1227–1239.
- Zeng, X., Zhang, Y., Nyström, A.M., 2012. Endocytic uptake and intracellular trafficking of bis-MPA-based hyperbranched copolymer micelles in breast cancer cells. *Biomacromolecules* 13, 3814–3822.